JACS
JOURNAL OF THE AMERICAN CHEMICAL SOCIETY
Communication
pubs.acs.org/JACS

Chemical Characterization of an Alkali-Like Superatom Consisting of a Ta-Encapsulating Si_{16} Cage

Masahiro Shibuta,[†,‡] Tsutomu Ohta,[‡] Masato Nakaya,[‡,§] Hironori Tsunoyama,[‡,§] Toyoaki Eguchi,[‡,§] and Atsushi Nakajima*[,†,‡,§]

[†]Keio Institute of Pure and Applied Science (KiPAS) and [‡]Department of Chemistry, Keio University, 3-14-1 Hiyoshi, Kohoku-ku, Yokohama 223-8522, Japan

[§]Nakajima Designer Nanocluster Assembly Project, JST-ERATO, 3-2-1 Sakado, Takatsu-ku, Kawasaki 213-0012, Japan

Supporting Information

ABSTRACT: Chemical characterization was performed for an alkali-like superatom consisting of a Ta-encapsulating Si_{16} cage, $Ta@Si_{16}$, deposited on a graphite substrate using X-ray photoelectron spectroscopy (XPS) to element-specifically clarify the local electronic structure of the cage atoms. The XPS spectra derived from Ta 4f and Si 2p core levels have been well modeled with a single chemical component, revealing the formation of a symmetric Si cage around the Ta atom in the deposited nanoclusters. On chemical treatments by heating or oxygen exposure, it is found that the deposited $Ta@Si_{16}$ is thermally stable up to 700 K and is also exceptionally less reactive toward oxygen compared to other Ta−Si nanoclusters, although some heat degradation and oxidation accompany the treatments. These results show the promising possibility of applying $Ta@Si_{16}$ as a building block to fabricate cluster-assembled materials consisting of naked nanoclusters.

Recently there has been notable progress in cluster science that has revealed a promising potential for opening up new avenues of material science based on organic and inorganic chemistry.[1−10] Following the discovery of carbon-based fullerene,[11] many synthetic and theoretical investigations have been conducted. In particular, metal (M)-encapsulating binary nanoclusters, such as $M@B_n$,[12] $M@Si_n$,[13−23] $M@Al_{12}$,[24,25] $M@Au_{12}$,[26] and $M@Sn_n$,[23,27] have attracted much attention.

The greatest advantage of the metal-atom encapsulating binary nanocluster is that their functionalities can be designed by selecting the species of encapsulating central atom while retaining the geometrical symmetry. Among them, metal-atom encapsulating Si_{16} cage nanoclusters of the $M@Si_{16}$ have been extensively investigated experimentally and theoretically, because they exhibit so-called magic number behavior in the gas phase,[13−23] and because they seem to have a close affinity for silicon-based electronic nanodevices.[14,20,28] The origin of the magic number behavior has been experimentally and theoretically interpreted using two factors of geometric stability resulting from high structural symmetry and electronic shell closure (68 electrons).[19] Since the electronic closure in $M@Si_{16}$ is satisfied by encapsulating group-4 atoms (M = Ti, Zr, and Hf) in the neutrals, $M@Si_{16}$ with group-3 (M = Sc, Y, and Lu) and group-5 (M = V, Nb, and Ta) atoms complete the 68 electron shells in the anion and cation forms, respectively.[15−19,21−23] This means that superatoms with halogen-, rare-gas-, and alkali-like natures can be fabricated by changing the central atom of $M@Si_{16}$. In these extensive discussions of the magic number behavior for $M@Si_{16}$, however, there have been a few experimental approaches to elucidate their chemical robustness even in the free gas phase.[17]

Such caged nanoclusters can be expected to act as a building block for nanocluster-assembled materials, the chemical robustness of the nanocluster being an important factor in successfully fabricating functional nanomaterials via the accumulation and aggregation of individual nanoclusters. One of the major strategies for nanocluster-assembled materials is the formation of a ligated nanocluster, in which an appropriate ligand protects the nanocluster core geometrically and electronically, to prevent from degradation of their intrinsic properties induced by aggregation of the nanoclusters. Ligand-free accumulation is another important route to form the nanocluster-assembled material, particularly as the properties of an assembly of naked nanoclusters are expected to be unsteady but revolutionary because of conserving their superatomic nature. This strategy has a promising potential to discover a novel property of the assembled nanoclusters owing to their superatomic interaction, which is attractive from the viewpoints of providing charge transport with lower energy dissipation and higher mobility.

In order to utilize the superatomic nanoclusters in a naked form for assembly into functional devices, they need to be deposited and immobilized onto a solid-state substrate. To perform the size selective isolation of the naked nanoclusters, magic numbered "ion" formation in the gas phase is a versatile tool to couple with mass spectrometry. The caged nanocluster of $Ta@Si_{16}^+$ is a good candidate to examine superatomic behavior to assemble themselves, because an ion signal of $TaSi_{16}^+$ (m/z = 630) prominently appears as magic numbers.[15,17] Indeed the deposition of $Ta@Si_{16}^+$ onto a substrate was examined by scanning probe microscopy/spectroscopy showing the physical properties of height and the HOMO−LUMO gap on several substrates,[29,30] but important chemical issues of their chemical states and stability are unknown for the functional assembled materials.

Here, we report that we have deposited $Ta@Si_{16}^+$ on a surface of highly oriented pyrolytic graphite (HOPG) and probed its chemical state and chemical stability by means of X-ray

Received: July 31, 2015
Published: October 29, 2015

DOI: 10.1021/jacs.5b08035
J. Am. Chem. Soc. 2015, 137, 14015−14018

photoelectron spectroscopy (XPS), which provides reliable information about chemical status of particular elements by measuring the energy positions of inner-core electrons. The result shows that the $Ta@Si_{16}$ deposited on the substrate maintains its metal-encapsulating framework even after thermal and chemical treatments, and further revealing the formation of spatially delocalized electronic states owing to the interaction between superatomic molecular orbitals.

$Ta@Si_{16}^{+}$ are synthesized by a magnetron sputtering method[31,32] and are deposited onto the cleaned HOPG substrate after being guided through ion optics and mass-selected with a quadrupole mass filter. Detailed experimental procedure is described in the Supporting Information.

Figure 1 shows XPS spectra (circles) measured around the (a) Si 2p and (b) Ta 4f core levels, where the background

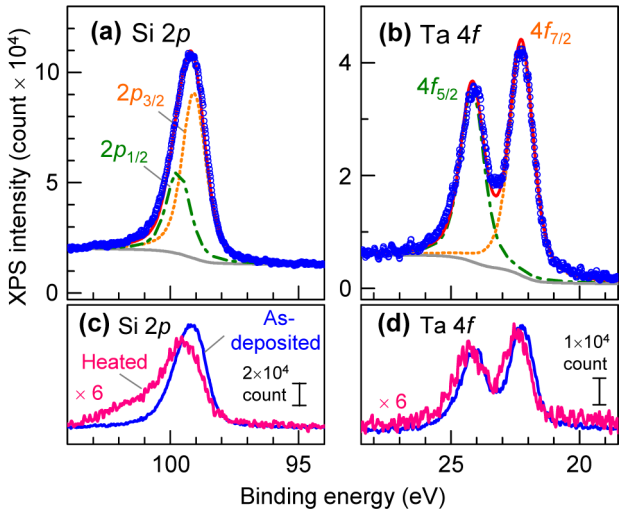

Figure 1. XPS spectra for $Ta@Si_{16}$ deposited on HOPG around (a) Si 2p and (b) Ta 4f core levels. The fitted results (red line) and spin−orbit contributions (orange dotted and green dash-dotted lines) are superimposed in (a) and (b). Background-subtracted XPS spectra of the $Ta@Si_{16}$ film for (c) Si 2p and (d) Ta 4f before and after heating (720 K, 16 h) are shown by blue and red lines, respectively.

component determined by the Shirley method is represented with a gray solid line. The ratio between the integrated intensity of Ta 4f and Si 2p is evaluated to be 1:1.58 that agrees well with the ratio calculated for $Ta@Si_{16}$ (1:1.53) using photoemission cross sections of Si 2p and Ta 4f.[33] To reveal more details, the spectra have been deconvoluted taking into account spin−orbit splitting whose energy separation and branching ratio are fixed at the literature values. The dotted and dashed-dotted lines in Figure 1a,b represent the component of Si $2p_{3/2}$ (Ta $4f_{7/2}$) and Si $2p_{1/2}$ (Ta $4f_{5/2}$), respectively. Parameters in the deconvolutions[34] are noted in the Supporting Information. As shown by the red lines, both levels are reproduced with a single chemical component indicating uniform chemical environments of Ta and Si. These results reveal that a symmetric Si cage is formed around the Ta atom as a metal-encapsulating cage structure of $Ta@Si_{16}$, i.e., 16 Si atoms are isotropically distributed around a central Ta atom.

The energy position of Si $2p_{3/2}$ (99.08 eV) is very close to the bulk value (99.2 eV),[35] while that of Ta $4f_{7/2}$ (22.26 eV) is about 0.6 eV larger than that of the bulk (21.6 eV).[36] Since energy positions of both core levels of Si 2p and Ta 4f are sensitive to the number of valence electrons (~1 eV shift per a valence electron),[37,38] the result indicates that Ta has a slight positive charge, while Si is almost neutral. In fact, the result implies that deposited $Ta@Si_{16}$ might be positively charged on the HOPG to satisfy a 68 electron shell closing, but it is hard to discuss the accurate charge state of individual $Ta@Si_{16}$ on HOPG with XPS. This is because the caged Si atoms themselves are negatively charged owing to larger electronegativity than Ta. Since the donated electron from the Ta atom is shared with 16 Si atoms, the amount of chemical shift in Si 2p is too small to determine the charge state.

As discussed below, our STM observations reveal that $Ta@Si_{16}$ deposited on HOPG accumulate into small islands. By analogy with alkali-metal atoms on graphite, the charge transfer would be much less in the accumulated clusters than the isolated ones, which is supported by our XPS results for $Ta@Si_{16}$ on C_{60} (see Supporting Information S4). Figure 2a,b shows an STM image

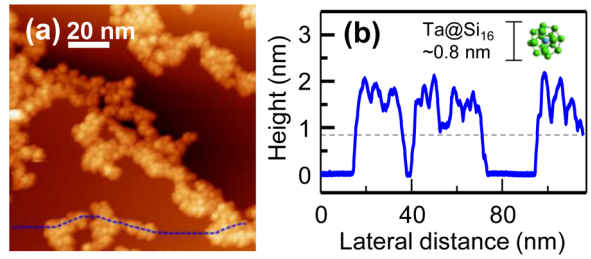

Figure 2. (a) An STM image (120 × 120 nm^2) of $Ta@Si_{16}$ deposited HOPG surface. Tip bias (V_{tip}) and current (I_t) are −2.3 V and 2 pA, respectively. (b) Height profile taken along a blue-dotted line in (a).

(120 × 120 nm^2) obtained from $Ta@Si_{16}$ deposited on a HOPG and a line profile taken along the broken line in the image. Island structures are formed and the islands consist of small dot-shaped components with a height of about 1 nm, which would correspond to individual $Ta@Si_{16}$. The results indicate that $Ta@Si_{16}$ can accumulate while keeping their superatomic properties, although they do not show ordered arrangements on HOPG. Since assembled structures are formed not only by their own interactions but also by surface/interface interactions, a HOPG seems less likely to form a $Ta@Si_{16}$ assembly.

Figure 1c,d shows the background-subtracted XPS spectra before and after heating at a temperature of 720 K for 16 h. After the heating, the Si 2p slightly shifted toward the higher binding energy (BE) (99.5 eV) and asymmetrically broadened on the higher BE side, while the shape of Ta 4f was almost unchanged. This suggests that the surrounding Si cage of $Ta@Si_{16}$ is somewhat altered by heating, perhaps by partially coalescing with HOPG or themselves, but the preserved cage prevents the Ta atoms from interacting with others. In fact, when surface Si atoms are bonded with carbon atoms in a defect of the HOPG, it has been reported that the Si 2p are shifted to higher energy to around 101.3 eV.[39] Furthermore, the broadening of Si 2p implies the formation of amorphous network of silicon atoms.[40] Importantly, on heating, the compositional ratio of Ta to Si atoms remains constant based on the XPS intensity, Si 2p:Ta 4f = 1:1.63, and therefore the cage surface of $Ta@Si_{16}$ seems to be partially fused, thereby retaining their individuality. In fact, after heating at a temperature around 400 K, the individual $Ta@Si_{16}$ are still discernible in the STM images for the aggregated islands (Figure S2). Furthermore, the heating lessens the intensity of each level to about 1/6, which indicates that the deposited nanoclusters aggregate, although it cannot be excluded that $Ta@Si_{16}$ itself might desorb from HOPG. This result may imply that

DOI: 10.1021/jacs.5b08035
J. Am. Chem. Soc. 2015, 137, 14015−14018

there is a benefit in choosing an appropriate solvent to perform the initial purification steps, because the heating causes the partial degradation of $Ta@Si_{16}$.

The above results show that $Ta@Si_{16}$ maintains its metal-encapsulating framework even after deposition onto HOPG, hence being expected to exhibit high chemical stability. In order to demonstrate this, the $Ta@Si_{16}$ deposited on the HOPG was exposed to oxygen, and its chemical state tracked by XPS. Figure 3a,b shows the XPS spectra around the Si 2p and Ta 4f levels

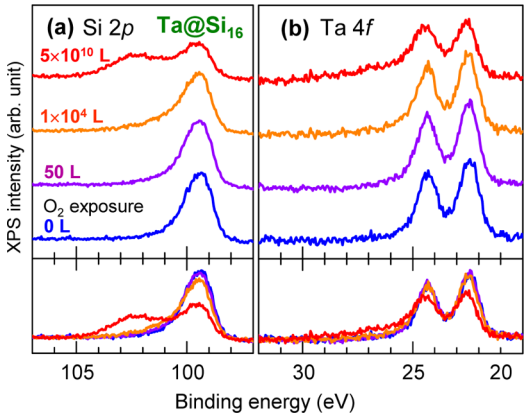

Figure 3. Normalized XPS spectra for $Ta@Si_{16}$ deposited on HOPG in (a) Si 2p and (b) Ta 4f levels, depending on oxygen exposures in the range $0-5 \times 10^{10}$ L, where the background are subtracted. For comparison, all series are superimposed in the bottom of each figure.

taken before and after oxygen exposure. Each spectrum is normalized by the total intensity after subtracting the background. Superimposed spectra normalized to the intensity are also shown at the bottom. The amount of oxygen exposure is noted in Langmuir, L (1 L = 1.33×10^{-4} Pa·s). For both levels, no significant difference is apparent below an exposure of 1×10^4 L. Even after exposing to 5×10^{10} L (0.1 MPa × 60 s) oxygen, the main components of Si 2p and Ta 4f stay at the energy positions of pristine $Ta@Si_{16}$, although additional components appear at higher BE of both levels, which can be attributed to the oxide of each element. Since it has been reported that surface atoms of bulk Si and Ta start to react with oxygen at much smaller dosages, <50 L,[37,41] our result clearly shows that $Ta@Si_{16}$ on HOPG has a very low reactivity toward oxygen.

Although $Ta@Si_{16}$ shows substantial resistance toward an O_2 adsorption reaction, it does eventually react to form oxides, and the $Ta@Si_{16}$ becomes markedly distorted. The O_2 exposure evolution of the Ta 4f peak is apparently slower than that of the Si 2p peak, suggesting that the surface Si of the cage is oxidized first, rather than the central Ta atom. Although the 1s peak of O atoms was observed at the BE of 532.5 eV, attributable to the oxidation states of O^{2-} (Figure S4),[37] no clear direct evidence for $(Ta@Si_{16})_2O$ formation was obtained that would signal the stoichiometric behavior of an alkali-like superatom.

For comparison, anions of $TaSi_3$ nanoclusters, which cannot have a metal-encapsulating structure, were deposited onto HOPG and exposed to oxygen. Figure 4a,b shows the XPS spectra around Si 2p and Ta 4f obtained from $TaSi_3$ deposited on HOPG for changing oxygen dosages. Both levels show much broader structures than that of $Ta@Si_{16}$. After exposing to 5×10^{10} L oxygen, clear peaks suggesting single chemical components appeared at the BE of 102.8 eV for Si 2p and 27.2 eV for Ta $4f_{7/2}$, which are close to those reported for a tantalum

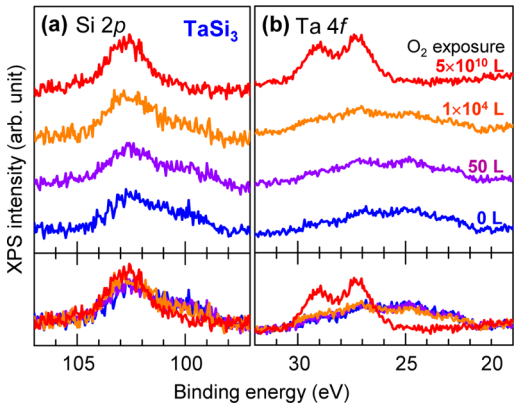

Figure 4. XPS spectra for $TaSi_3$ deposited on HOPG in (a) Si 2p and (b) Ta 4f levels under the same condition as Figure 3a,b, depending on oxygen exposures in the range $0-5 \times 10^{10}$ L. For comparison, all series of spectra are superimposed in the bottom of each figure.

disilicide ($TaSi_2$) film oxidized by exposing to air.[38] This result suggests that some of the $TaSi_3$ deposited on HOPG was already oxidized before oxygen exposure experiments. In fact, by XPS measurements, an O 1s signal is detected on a $TaSi_3$ deposited HOPG, whereas it is hardly observed on $Ta@Si_{16}$ film, as shown in Figure S5. The oxidation of $TaSi_3$ during the synthesis and/or deposition could be caused by oxygen impurity contained in the Ar and He gases used to synthesize nanoclusters, because the concentration of residual oxygen (<0.01 ppm by volume) might be sufficient to oxidize $TaSi_3$ even in the vacuum sample preparation. The above result clearly elucidates that $Ta@Si_{16}$ acquire a high chemical stability against oxidation owing to its metal-encapsulating framework.

As well as XPS, ultraviolet photoemission spectroscopy (UPS) is a powerful technique to investigate valence electronic states. However, performing UPS with 21.22 eV photons for deposited $Ta@Si_{16}$ exhibits no distinct peaks assignable to the electronic states of $Ta@Si_{16}$ either on HOPG or on C_{60}/HOPG, as shown in Figure 5. With the deposition of $Ta@Si_{16}$ onto C_{60}/HOPG,

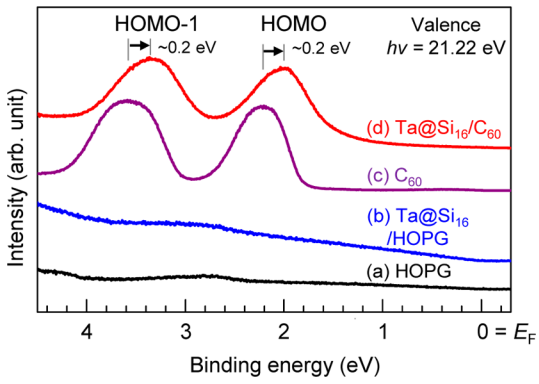

Figure 5. Valence (UPS) spectra for (a) HOPG, (b) $Ta@Si_{16}$ film/HOPG, (c) C_{60} monolayer, and (d) $Ta@Si_{16}$ film on C_{60} monolayer.

the C_{60}-derived peaks show a small energy shift of 0.2 eV toward the Fermi level and a new broad component in the low-energy region. Since similar spectral changes have been observed in the UPS spectra for a sodium (Na)-doped C_{60} film,[42] the spectral changes may suggest the alkali-like superatom behavior of $Ta@Si_{16}$. Recently, Claes et al. studied the infrared multiple photon dissociation (IR-MPD) spectrum of $Si_{16}V^+$ and reported that the

DOI: 10.1021/jacs.5b08035
J. Am. Chem. Soc. 2015, 137, 14015−14018

IR-MPD spectrum is very different from those of other Si_nV^+ (n = 12−15).[21] It shows no distinct, narrow absorption peaks but has a couple of broad features. Using a molecular dynamics simulation, indeed, they suggest that $Si_{16}V^+$ is dynamic, undergoing rapid transitions between nearly degenerate local minima. The dynamic behavior for $Si_{16}V^+$ might be consistent with no distinct peaks in the UPS in this study because fluctuating structures of $Si_{16}Ta^+$ would not exhibit any stationary electronic states.

To conclude, we have evaluated the chemical states and stability of $Ta@Si_{16}$ deposited on a HOPG by XPS, revealing a uniform chemical state of the relevant elements. Combining these data with evidence of a low reactivity toward oxygen exposure proves that the metal-encapsulating cage of $Ta@Si_{16}$ has been maintained after deposition onto the substrate, a situation which is also supported by the STM. The chemical robustness of $M@Si_{16}$ nanoclusters will enable us to construct novel devices utilizing their unique properties as superatoms. We expect these experimental findings to greatly contribute to the opening up of a new field of nanomaterial science based on superatom assembly through functionalities that emerge from an atomic scale interaction among naked superatomic nanoclusters.

■ ASSOCIATED CONTENT

Supporting Information

The Supporting Information is available free of charge on the ACS Publications website at DOI: 10.1021/jacs.5b08035.

Mass spectrum of Ta_mSi_n, fitting procedures, XPS results of $Ta@Si_{16}$ on C_{60} film and of O 1s core level, and STM images (PDF)

■ AUTHOR INFORMATION

Corresponding Author

*nakajima@chem.keio.ac.jp

Notes

The authors declare no competing financial interest.

■ ACKNOWLEDGMENTS

This work is partly supported by JSPS KAKENHI of Grant-in-Aids for Young Scientists (B) grant no. 25810010 and for Scientific Research (A) grant no. 15H02002. T.O. thanks a financial support from Grant-in-Aid for JSPS Fellows.

■ REFERENCES

(1) Khanna, S. N.; Jena, P. *Phys. Rev. Lett.* **1992**, *69*, 1664−1667.
(2) Crooks, R. M.; Zhao, M.; Sun, L.; Chechik, V.; Yeung, L. K. *Acc. Chem. Res.* **2001**, *34*, 181−190.
(3) Zheng, J.; Dickson, R. M. *J. Am. Chem. Soc.* **2002**, *124*, 13982−13983.
(4) Darling, S. B.; Yufa, N. A.; Cisse, A. L.; Bader, S. D.; Sibener, S. J. *Adv. Mater.* **2005**, *17*, 2446−2450.
(5) Castleman, A. W.; Jena, P. *Proc. Natl. Acad. Sci. U. S. A.* **2006**, *103*, 10554−10559.
(6) Claridge, S. A.; Castleman, A. W., Jr.; Khanna, S. N.; Murray, C. B.; Sen, A.; Weiss, P. S. *ACS Nano* **2009**, *3*, 244−255.
(7) Castleman, A. W., Jr.; Khanna, S. N. *J. Phys. Chem. C* **2009**, *113*, 2664−2675.
(8) Jin, R. *Nanoscale* **2010**, *2*, 343−362.
(9) Jang, Y. H.; Chung, K.; Quan, L. N.; Špačková, B.; Šipová, H.; Moon, S.; Cho, W. J.; Shin, H.-Y.; Jang, Y. J.; Lee, J.-E.; Kochuveedu, S.; Th; Yoon, M. J.; Kim, J.; Yoon, S.; Kim, J. K.; Kim, D.; Homolab, J.; Kim, D. H. *Nanoscale* **2013**, *5*, 12261−12271.
(10) Roy, X.; Lee, C.-H.; Crowther, A. C.; Schenck, C. L.; Besara, T.; Lalancette, R. A.; Siegrist, T.; Stephens, P. W.; Brus, L. E.; Kim, P.; Steigerwald, M. L.; Nuckolls, C. *Science* **2013**, *341*, 157−160.
(11) Kroto, H. W.; Heath, J. R.; O'Brien, S. C.; Curl, R. F.; Smalley, R. E. *Nature* **1985**, *318*, 162−163.
(12) Zhai, H.-J.; Zhao, Y.-F.; Li, W.-L.; Chen, Q.; Bai, H.; Hu, H.-S.; Piazza, Z. A.; Tian, W.-J.; Lu, H.-G.; Wu, Y.-B.; Mu, Y.-W.; Wei, G.-F.; Liu, Z.-P.; Li, J.; Li, S.-D.; Wang, L.-S. *Nat. Chem.* **2014**, *6*, 727−731.
(13) Beck, S. M. *J. Chem. Phys.* **1989**, *90*, 6306−6312.
(14) Kumar, V.; Kawazoe, Y. *Phys. Rev. Lett.* **2001**, *87*, 045503.
(15) Koyasu, K.; Akutsu, M.; Mitsui, M.; Nakajima, A. *J. Am. Chem. Soc.* **2005**, *127*, 4998−4999.
(16) Reveles, J. U.; Khanna, S. N. *Phys. Rev. B: Condens. Matter Mater. Phys.* **2006**, *74*, 035435.
(17) Koyasu, K.; Atobe, J.; Akutsu, M.; Mitsui, M.; Nakajima, A. *J. Phys. Chem. A* **2007**, *111*, 42−49.
(18) Torres, M. B.; Fernández, E. M.; Balbás, L. C. *Phys. Rev. B: Condens. Matter Mater. Phys.* **2007**, *75*, 205425.
(19) Lau, J. T.; Hirsch, K.; Klar, Ph.; Langenberg, A.; Lofink, F.; Richter, R.; Rittmann, J.; Vogel, M.; Zamudio-Bayer, V.; Möller, T.; von Issendorff, B. *Phys. Rev. A: At., Mol., Opt. Phys.* **2009**, *79*, 053201.
(20) Cantera-López, H.; Balbás, L. C.; Borstel, G. *Phys. Rev. B: Condens. Matter Mater. Phys.* **2011**, *83*, 075434.
(21) Claes, P.; Janssens, E.; Ngan, V. T.; Gruene, P.; Lyon, J. T.; Harding, D. J.; Fielicke, A.; Nguyen, M. T.; Lievens, P. *Phys. Rev. Lett.* **2011**, *107*, 173401.
(22) Lau, J. T.; Vogel, M.; Langenberg, A.; Hirsch, K.; Rittmann, J.; Zamudio-Bayer, V.; Möller, T.; von Issendorff, B. *J. Chem. Phys.* **2011**, *134*, 041102.
(23) Atobe, J.; Koyasu, K.; Furuse, S.; Nakajima, A. *Phys. Chem. Chem. Phys.* **2012**, *14*, 9403−9410.
(24) Nakajima, A.; Kishi, T.; Sugioka, T.; Kaya, K. *Chem. Phys. Lett.* **1991**, *187*, 239−244.
(25) Li, X.; Wang, L. S. *Phys. Rev. B: Condens. Matter Mater. Phys.* **2002**, *65*, 153404.
(26) Zhai, H.-J.; Li, J.; Wang, L.-S. *J. Chem. Phys.* **2004**, *121*, 8369.
(27) Cui, L.-F.; Huang, X.; Wang, L.-M.; Li, J.; Wang, L.-S. *Angew. Chem.* **2007**, *119*, 756−759.
(28) Iwasa, T.; Nakajima, A. *J. Phys. Chem. C* **2012**, *116*, 14071−14077.
(29) Nakaya, M.; Iwasa, T.; Tsunoyama, H.; Eguchi, T.; Nakajima, A. *Nanoscale* **2014**, *6*, 14702−14707.
(30) Nakaya, M.; Iwasa, T.; Tsunoyama, H.; Eguchi, T.; Nakajima, A. *J. Phys. Chem. C* **2015**, *119*, 10962−10968.
(31) Tsunoyama, H.; Zhang, C.; Akatsuka, H.; Sekiya, H.; Nagase, T.; Nakajima, A. *Chem. Lett.* **2013**, *42*, 857−859.
(32) Zhang, C.; Tsunoyama, H.; Akatsuka, H.; Sekiya, H.; Nagase, T.; Nakajima, A. *J. Phys. Chem. A* **2013**, *117*, 10211−10217.
(33) Scofield, J. H. *J. Electron Spectrosc. Relat. Phenom.* **1976**, *8*, 129−137.
(34) Ohta, T.; Shibuta, M.; Tsunoyama, H.; Negishi, Y.; Eguchi, T.; Nakajima, A. *J. Phys. Chem. C* **2013**, *117*, 3674−3679.
(35) Rangelov, G.; Fauster, Th. *Surf. Sci.* **1996**, *365*, 403−410.
(36) Riffe, D. M.; Wertheim, G. K. *Phys. Rev. B: Condens. Matter Mater. Phys.* **1993**, *47*, 6672−6679.
(37) Hollinger, G.; Morar, J. F.; Himpsel, F. J.; Hughes, G.; Jordan, J. L. *Surf. Sci.* **1986**, *168*, 609−616.
(38) Thomas, J. H., III; Hammer, L. H. *J. Electrochem. Soc.* **1989**, *136*, 2004−2010.
(39) Kusunoki, I.; Igari, Y. *Appl. Surf. Sci.* **1992**, *59*, 95−104.
(40) Ley, L.; Reichardt, J.; Jonson, R. L. *Phys. Rev. Lett.* **1982**, *49*, 1664−1667.
(41) van der Veen, J. F.; Himpsel, F. J.; Eastman, D. E. *Phys. Rev. B: Condens. Matter Mater. Phys.* **1982**, *25*, 7388−7397.
(42) Gu, C.; Stepniak, F.; Poirier, D. M.; Jost, M. B.; Benning, P. J.; Chen, Y.; Ohno, T. R.; José Luís Martins, J. L.; Weaver, J. H.; Fure, J.; Smalley, R. E. *Phys. Rev. B: Condens. Matter Mater. Phys.* **1992**, *45*, 6348.

DOI: 10.1021/jacs.5b08035
J. Am. Chem. Soc. 2015, 137, 14015−14018